Phase Equilibria and Thermodynamic Properties of Selected Compounds in the Ag–Ga–S–AgBr System for Modern Application in Energy Conversion Devices

Mykola Moroz, Fiseha Tesfaye, Pavlo Demchenko, Myroslava Prokhorenko, Bohdan Rudyk, Orest Pereviznyk, Emanuela Mastronardo, Daniel Lindberg, Oleksandr Reshetnyak, and Leena Hupa

Abstract The phase equilibria of the Ag–Ga–S–AgBr system in the part GaS–Ga_2S_5–AgBr–Ag_2S below 600 K were investigated by the modified electromotive force (EMF) method using the Ag^+ catalysts as small nucleation centers of equilibrium phases. Division of the GaS–Ga_2S_5–AgBr–Ag_2S was carried out with the participation of the following compounds Ag_2S, GaS, Ga_2S_3, AgBr, Ag_9GaS_6, $AgGaS_2$, Ag_3SBr, $Ag_3Ga_2S_4Br$, and $Ag_{27}Ga_2S_{12}Br_9$. Reactions were performed by applying electrochemical cells (ECs) with the structure: (−) IE | NE | SSE | R{Ag^+} | PE | IE (+), where IE is the inert electrode (graphite powder), NE is the negative electrode

M. Moroz (✉) · B. Rudyk
Department of Chemistry and Physics, National University of Water and Environmental Engineering, Rivne 33028, Ukraine
e-mail: m.v.moroz@nuwm.edu.ua

F. Tesfaye · L. Hupa
Johan Gadolin Process Chemistry Centre, Åbo Akademi University, 20500 Turku, Finland

P. Demchenko
Department of Inorganic Chemistry, Ivan Franko National University of Lviv, Lviv 79005, Ukraine

M. Prokhorenko
Department of Cartography and Geospatial Modeling, Lviv Polytechnic National University, Lviv 79013, Ukraine

O. Pereviznyk · O. Reshetnyak
Department of Physical and Colloid Chemistry, Ivan Franko National University of Lviv, Lviv 79005, Ukraine

E. Mastronardo
Department of Engineering, University of Messina, 98166 Messina, Italy

D. Lindberg
Department of Chemical and Metallurgical Engineering, Aalto University, Kemistintie 1, 02150 Espoo, Finland

C. Iloeje et al. (eds.), *Energy Technology 2024*, The Minerals, Metals & Materials Series, https://doi.org/10.1007/978-3-031-50244-6_23

(silver powder), SSE is the solid-state electrolyte (glassy Ag_3GeS_3Br), PE is the positive electrode, R{Ag^+} is the region of Ag^+ diffusion into PE. The measured EMF and temperature values of ECs were used to determine the standard thermodynamic functions of the compounds $Ag_3Ga_2S_4Br$ and $Ag_{27}Ga_2S_{12}Br$.

Keywords Photovoltaic compounds · Phase equilibria · Thermodynamic properties · EMF method · Gibbs energy

Introduction

To date, establishing the phase composition of the equilibrium *T-x* space of multicomponent inorganic systems at $T \leq 600$ K, when there are kinetic obstacles to achieving a state of thermodynamic equilibrium, remains relevant. The effect on samples of such external factors as long-term annealing during temperature and pressure variations is ineffective in many cases. The possibility of overcoming such kinetic obstacles was established in Refs. [1, 2]. For this purpose, the silver ions Ag^+ were used as catalysts, i.e., small nucleation centers of equilibrium phases.

The concentration tetrahedra of the Ag–Ga–X–Y (X = S, Se, Te; Y = Cl, Br, I) in part of the quasi-ternary Ag_2X–Ga_2X_3–AgY systems are characterized by the presence of semiconductor compounds of the formula composition $AgGa_2X_3Y$ (structure type $CuIn_2Te_3Cl$, space group I–4) [3]. Quaternary compounds decompose upon annealing at 600 K [4].

For the case X = S and Y = Br, the quasi-ternary Ag_2S–Ga_2S_3–AgBr system, in addition to the quaternary compound $AgGa_2S_3Br$, is characterized by the following ternary phases Ag_9GaS_6, $AgGaS_2$ (quasi-binary system Ag_2S–Ga_2S_3) and Ag_3SBr (quasi-binary system Ag_2S–AgBr) [5, 6]. The solid-state phase equilibria in the Ag–Ga–S system and thermodynamic properties of ternary phases were reported in Ref. [7]. The argyrodite family compound Ag_9GaS_6 is a promising thermoelectric material with the figure of merit parameter $ZT \sim 0.6$ and has intrinsic ultralow lattice thermal conductivity [8]. Moreover, Ag_9GaS_6 has a high silver ionic conductivity [9, 10]. The $AgGaS_2$ belongs to the chalcopyrite-structured ternary semiconductor compounds with a direct band gap of (2.48–2.75) eV. This compound has a high transparency in the mid-IR range and can be used as a commercial material for photovoltaic and nonlinear optical applications as well as a promising candidate for X-ray dosimetry [11–13]. The Ag_3SBr compound belongs to the class of superionic materials [14]. Thus, the multi-component compounds and solid solutions based on phases of the Ag–Ga–S system have been considered interesting scientific objects due to the diversity of their crystal structures and physicochemical properties [15–19]. However, these compounds no longer fully meet all the requirements of a new generation of devices for modern applications. For example, the band gap value and weak absorption in the visible light region limit the use of $AgGaS_2$ as absorber material for photovoltaic solar cells. Recently, the photo-electrochemical cells based on the $AgGaS_2$ compound showed an efficiency of 5.85% [20]. Optimization technology for the synthesis of new materials and improving their technical characteristics is impossible without a comprehensive analysis of the thermodynamic properties of intermediate phases and construction equilibrium phase diagrams.

The points of intersection of the cross-sections $AgGaS_2$–AgBr and Ag_9GaS_6–AgBr of the quasi-ternary system with the tie-line Ga_2S_3–Ag_3SBr are places of potential formation of quaternary compounds $Ag_3Ga_2S_4Br$ and $Ag_{27}Ga_2S_{12}Br_9$. There are no previous reports on quaternary compounds of mentioned composition. The thermodynamic conditions for the formation of quaternary phases likely correspond to the temperature values $T < 600$ K, where there are kinetic obstacles to such a process.

The purpose of this work was to establish by the electromotive force (EMF) method the phase composition of the Ga_2S_3–Ag_3SBr cross-section of the Ag_2S–Ga_2S_3–AgBr system below 600 K and to determine the values of the standard thermodynamic functions of the quaternary compounds in the system. The two-phase equilibrium between compounds of the $AgGaS_2$–$Ag_3Ga_2S_4Br$ and Ag_9GaS_6–$Ag_{27}Ga_2S_{12}Br_9$ cross-sections can be used to vary the nonlinear optical properties of the phases in the way of forming solid solutions on a mutual basis.

Experimental

The high-purity substances Ag (> 99.9 wt%, Alfa Aesar, Germany), Ga, and S (> 99.99 wt%, Alfa Aesar, Germany) were used to synthesize the binary compounds Ag_2S, GaS, and Ga_2S_3. Melts of the Ag_2S, GaS, and Ga_2S_3 compounds in an inert atmosphere were cooled to room temperature, then crushed to a particle size of ~ 1×10^{-6} m for preparation of the positive electrodes (PE) of electrochemical cells (ECs) [21, 22].

The modified EMF method [1, 2] was used both to establish the phase equilibria in the GaS–Ga_2S_5–AgBr–Ag_2S part of the Ag–Ga–S–AgBr concentration tetrahedron below 600 K and to determine the thermodynamic parameters of compounds. For these investigations, a certain number of ECs were assembled:

$$(-)\ \mathrm{IE|NE|SSE|R}\left\{\mathrm{Ag}^{+}\right\}\mathrm{|PE|IE}(+),$$

where IE is the inert electrode (graphite powder), NE is the negative electrode (silver powder), SSE is the solid-state electrolyte (glassy Ag_3GeS_3Br [23]), and R{Ag^+} is the region of PE that contacts with SSE. At the stage of cell preparation, PE is the non-equilibrium phase mixture of the well-mixed powdered binary compounds Ag_2S, GaS, Ga_2S_3, and AgBr (99.5 wt%, Alfa Aesar, Germany). Compositions of these mixtures covered the entire concentration space of the GaS–Ga_2S_5–AgBr–Ag_2S region. An equilibrium set of phases was formed in the R{Ag^+} region at 600 K for 48 h. The Ag^+ ions, displaced for thermodynamic reasons from the NE to the PE electrodes of the ECs, acted as catalysts, i.e., small nucleation centers of equilibrium phases [21, 22].

The experiments were performed in a resistance furnace described in Ref. [24, 25]. To assemble the ECs, a fluoroplastic base with a hole with a diameter of 2 mm was used. The powder components of ECs were pressed at pressure 10^8 Pa into the hole under a load of (2.0 ± 0.1) tons to a density of $\rho = (0.93 \pm 0.02)\ \rho_0$, where ρ_0 is the experimentally determined density of cast samples. The assembled cells were placed in a quartz tube with nozzles for the purging of argon gas [26, 27]. The argon gas had a direction from the NE to PE of ECs at the rate of (10.0 ± 0.2) cm^3 min^{-1}. The temperature of ECs was maintained by an electronic thermostat with ± 0.5 K accuracy. A Picotest M3500A digital voltmeter with an input impedance of > 10^{12} Ohms was used to measure the EMF (E) values of the cells (accuracy ± 0.3 mV) at different temperatures. The reproducibility of the E versus T dependences of ECs in heating–cooling cycles was a criterion for completing the formation of the equilibrium set of phases in the R{Ag^+} region [28].

Results and Discussion

The division of the concentration tetrahedron Ag–Ga–S–AgBr into separate four-phase regions in the GaS–Ga_2S_5–AgBr–Ag_2S part below 600 K is shown in Fig. 1. The division was carried out based on the experimental results of the E versus T relations of the ECs with PE of different phase regions and taking into account the basic rules of the EMF method [29–31]:

(1) within a specific phase region, the EMF value of the cell does not depend on the phase composition of the PE;
(2) ECs with PE of different phase regions are characterized by different EMF values at T = const, Table 1;

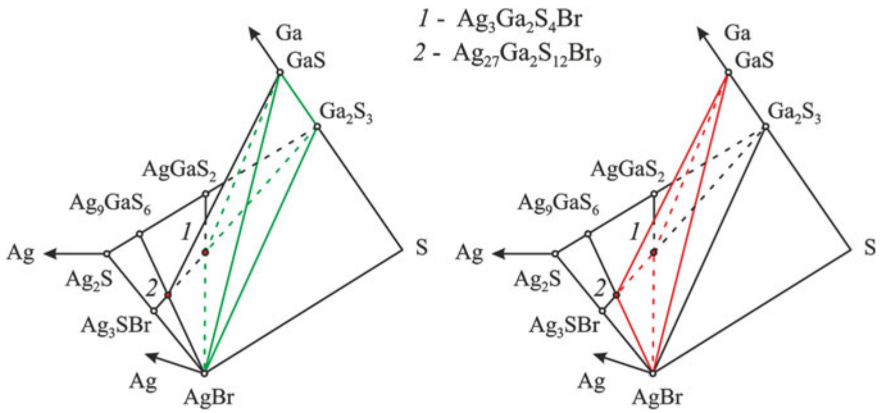

Fig. 1 Spatial position of tetrahedra GaS–Ga_2S_3–AgBr–$Ag_3Ga_2S_4Br$ (left) and GaS–AgBr–$Ag_{27}Ga_2S_{12}Br_9$–$Ag_3Ga_2S_4Br$ (right) in the concentration space of the Ag–Ga–S–AgBr system

Table 1 Measured values of temperature (T) and EMF (E) of the ECs with PE of different phase regions at pressure $P = 10^5$ Pa

T/K	Phase regions		T/K	Phase regions	
	(I)	(II)		(I)	(II)
	E/mV	E/mV		E/mV	E/mV
390.4	211.1	204.1	420.5	224.3	209.4
395.4	213.4	204.9	425.4	226.6	210.2
400.4	215.4	205.9	430.4	228.8	211.2
405.4	217.7	206.8	435.3	231.1	212.1
410.4	219.8	207.6	440.4	233.4	212.9
415.4	222.2	208.5	445.4	235.5	213.7

Standard uncertainties u are $u(T) = 0.5$ K, $u(P) = 10^4$ Pa, and $u(E) = 0.3$ mV

(3) the four-phase region further away from the figurative point of Ag is characterized by a higher EMF value at a specific temperature, Fig. 2.

The spatial position of the established four-phase regions $GaS–Ga_2S_3–AgBr–Ag_3Ga_2S_4Br$ (phase region (I)) and $GaS–AgBr–Ag_{27}Ga_2S_{12}Br_9–Ag_3Ga_2S_4Br$ (phase region (II)) relative to the silver point was used to establish the overall potential-determining reactions:

$$2Ag + 2Ga_2S_3 + AgBr = Ag_3Ga_2S_4Br + 2GaS, \quad (R1)$$

$$8Ag + 5Ag_3Ga_2S_4Br + 4AgBr = Ag_{27}Ga_2S_{12}Br_9 + 8GaS. \quad (R2)$$

Reactions (R1) and (R2) were carried out in the PE of ECs, and the phase mixtures correspond to phase regions (I) and (II), respectively. According to reactions (R1)

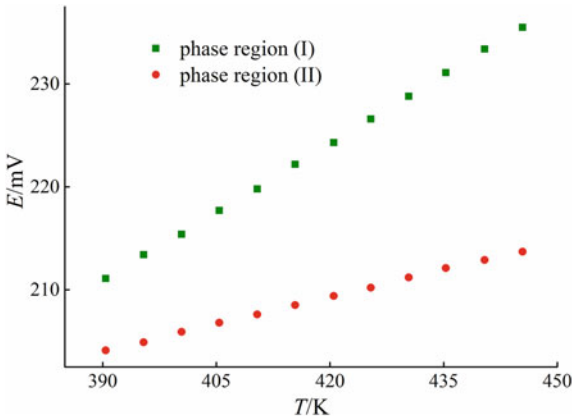

Fig. 2 E versus T dependencies of the ECs with PE of the phase regions (I) and (II)

and (R2), the ratios of binary compounds for assembling the PE of ECs were established. In particular, the compounds $Ag_3Ga_2S_4Br$ and $Ag_{27}Ga_2S_{12}Br_9$ are present in the PE compositions in the following ratios of mixtures of the binary compounds: Ag_2S:Ga_2S_3:AgBr = 1:1:1 and Ag_2S:Ga_2S_3:AgBr = 9:1:9, respectively.

From the data analysis of Fig. 2, it follows that the E versus T dependencies of the ECs in the phase regions (I) and (II) are linear. Therefore, the results of EMF measurements processed by the least squares method [32] can be presented in the form of Eq. (1):

$$E = a + bT \equiv \overline{E} + b\left(T - \overline{T}\right), \tag{1}$$

where $\overline{E} = \frac{\sum E_i}{n}$, $\overline{T} = \frac{\sum T_i}{n}$ (E_i is the EMF of the cell at temperature T_i; n is a number of experimental pairs E_i and T_i).

Coefficients a and b were calculated by the following Eqs. (2) and (3):

$$a = \overline{E} - b\overline{T}, \tag{2}$$

$$b = \frac{\sum\left[\left(E_i - \overline{E}\right)\left(T_i - \overline{T}\right)\right]}{\sum\left(T_i - \overline{T}\right)^2}. \tag{3}$$

The statistical dispersions of the measurement uncertainties consisted of the calculation variances of experimental values of EMF E (u_E^2), coefficients b (u_b^2) and a (u_a^2), as well as dispersions of the calculated by Eq. (1) EMF values $\tilde{E}$ ($u_{\tilde{E}}^2$):

$$u_E^2 = \frac{\sum\left(E_i - \tilde{E}_i\right)^2}{n-2}, \tag{4}$$

$$u_b^2(T) = \frac{u_E^2}{\sum\left(T_i - \overline{T}\right)^2}, \tag{5}$$

$$u_a^2(T) = \frac{u_E^2}{n} + \frac{u_E^2\overline{T}^2}{\sum\left(T_i - \overline{T}\right)^2}, \tag{6}$$

$$u_{\tilde{E}}^2(T) = \frac{u_E^2}{n} + u_b^2\left(T - \overline{T}\right)^2. \tag{7}$$

Uncertainties (Δ_i) of the corresponding quantities can be calculated by the Eq. (8):

$$\Delta_i = k_{St}u_i \tag{8}$$

where k_{St} is the Student's coefficient, and u_i is the standard deviation. At the confidence level of 95% and $n = 12$, the Student's coefficient is equal $k_{St} = 2.179$ [32].

According to [33, 34], the final equation of the E versus T dependences together with the statistical dispersions can be expressed as:

$$E = a + bT \pm k_{St}\sqrt{\left(\frac{u_E^2}{n} + u_b^2\left(T - \overline{T}\right)^2\right)}. \quad (9)$$

An example of calculating the coefficients of Eq. (9) for the phase region (I) is given in Table 2.

Analogously to the phase region (I), coefficients E versus T dependence of the cell with PE of the phase region (II) were calculated. The results of the calculations are listed in Table 3.

The Gibbs energies ($\Delta_r G$), enthalpies ($\Delta_r H$), and entropies ($\Delta_r S$) of the reactions (R1) and (R2) were calculated by the following thermodynamic equations:

$$\Delta_r G = -zFE, \quad (10)$$

$$\Delta_r H = -zF[E - (dE/dT)T], \quad (11)$$

Table 2 Coefficients of the E versus T dependence of the cell with PE of the phase region (I)

T_i	E_i	$(T_i - \overline{T})$	$(T_i - \overline{T})^2$	$\tilde{E}_i$	$(E_i - \tilde{E}_i)$	$(E_i - \tilde{E}_i)^2$
K	mV	K	K^2	mV	mV	mV^2
390.4	211.1	– 27.50	756.25	211.04	0.06	0.00
395.4	213.4	– 22.50	506.25	213.26	0.14	0.02
400.4	215.4	– 17.50	306.25	215.49	– 0.09	0.01
405.4	217.7	– 12.50	156.25	217.71	– 0.01	0.00
410.4	219.8	– 7.50	56.25	219.94	– 0.14	0.02
415.4	222.2	– 2.50	6.25	222.17	0.03	0.00
420.5	224.3	2.60	6.76	224.44	– 0.14	0.02
425.4	226.6	7.50	56.25	226.62	– 0.02	0.00
430.4	228.8	12.50	156.25	228.84	– 0.04	0.00
435.3	231.1	17.40	302.76	231.02	0.08	0.01
440.4	233.4	22.50	506.25	233.29	0.11	0.01
445.4	235.5	27.50	756.25	235.52	– 0.02	0.00
$\overline{T} =$ 417.90	$\overline{E} =$ 223.28	–	$\sum(T_i - \overline{T})^2 =$ 3572.02	–	–	$\sum(E_i - \tilde{E}_i)^2 =$ 0.09

$\overline{T}$ is the average temperature value, $\tilde{E}$ is the EMF of the cell calculated according to Eq. (1)

Table 3 Coefficients and statistical dispersions of the E versus T dependencies of the ECs in the phase regions (I) and (II)

Phase regions	$E = a + bT \pm k_{St}\sqrt{\left(\frac{u_E^2}{n} + u_b^2(T - \overline{T})^2\right)}$
(I)	$E = 37.25 + 445.15 \times 10^{-3}T \pm 2.179\sqrt{\left(\frac{8.95\times10^{-3}}{12} + 2.51 \times 10^{-6}(T - 417.90)^2\right)}$
(II)	$E = 135.35 + 176.09 \times 10^{-3}T \pm 2.179\sqrt{\left(\frac{3.52\times10^{-3}}{12} + 9.86 \times 10^{-7}(T - 417.90)^2\right)}$

Table 4 Values of standard thermodynamic function of the reactions (R1) and (R2)

Reactions	$-\Delta_r G^\circ$	$-\Delta_r H^\circ$	$\Delta_r S^\circ$
	kJ mol^{-1}		J (mol K)$^{-1}$
(R1)	32.79 ± 0.08	7.19 ± 0.28	85.90 ± 0.66
(R2)	144.98 ± 0.20	104.47 ± 0.70	135.92 ± 1.67

Uncertainties for $\Delta_r G^\circ$, $\Delta_r H^\circ$, and $\Delta_r S^\circ$ are standard uncertainties

$$\Delta_r S = z\,F(\mathrm{d}E/\mathrm{d}T). \tag{12}$$

where z is the number of electrons involved in the reactions (R1) and (R2), F is the Faraday's constant, and E is the EMF of the ECs.

The values of the thermodynamic functions of reactions (R1) and (R2) in the standard state (T = 298 K and $P = 10^5$ Pa) were calculated according to Eqs. (10)–(12) and are listed in Table 4.

The Gibbs energy, enthalpy, and entropy of the reaction (R1) are related to the Gibbs energy, enthalpy, and entropy of the compounds Ga_2S_3, AgBr, $Ag_3Ga_2S_4Br$, GaS, and pure substance Ag by the following equations:

$$\Delta_{r(R1)}G^\circ = \Delta_f G^\circ_{Ag_3Ga_2S_4Br} + 2\Delta_f G^\circ_{GaS} - 2\Delta_f G^\circ_{Ga_2S_3} - \Delta_f G^\circ_{AgBr}, \tag{13}$$

$$\Delta_{r(R1)}H^\circ = \Delta_f H^\circ_{Ag_3Ga_2S_4Br} + 2\Delta_f H^\circ_{GaS} - 2\Delta_f H^\circ_{Ga_2S_3} - \Delta_f H^\circ_{AgBr}, \tag{14}$$

$$\Delta_{r(R1)}S^\circ = S^\circ_{Ag_3Ga_2S_4Br} + 2S^\circ_{GaS} - 2S^\circ_{Ag} - 2S^\circ_{Ga_2S_3} - S^\circ_{AgBr}. \tag{15}$$

It follows from Eqs. (13)–(15) that:

$$\Delta_f G^\circ_{Ag_3Ga_2S_4Br} = 2\Delta_f G^\circ_{Ga_2S_3} + \Delta_f G^\circ_{AgBr} - 2\Delta_f G^\circ_{GaS} + \Delta_{r(R1)}G^\circ, \tag{16}$$

$$\Delta_f H^\circ_{Ag_3Ga_2S_4Br} = 2\Delta_f H^\circ_{Ga_2S_3} + \Delta_f H^\circ_{AgBr} - 2\Delta_f H^\circ_{GaS} + \Delta_{r(R1)}H^\circ, \tag{17}$$

$$S^{\circ}_{Ag_3Ga_2S_4Br} = 2S^{\circ}_{Ag} + 2S^{\circ}_{Ga_2S_3} + S^{\circ}_{AgBr} - 2S^{\circ}_{GaS} + \Delta_{r(R1)}S^{\circ}. \tag{18}$$

Reactions to determine the standard thermodynamic properties $\Delta_f G^{\circ}$, $\Delta_f H^{\circ}$, and S° of the $Ag_{27}Ga_2S_{12}Br_9$ compound were written in similarity using (R2) with the corresponding stoichiometric numbers.

For the first time, the standard thermodynamic quantities of the quaternary compounds of the Ag–Ga–S–AgBr system were determined using Eqs. (16)–(18) and thermodynamic data of pure substances (Ag, Ga, S, Br_2) and the binary compound GaS, Ga_2S_3, AgBr [35]. The results of the calculations are listed in Table 5.

The temperature dependences of the Gibbs energies of formations of the quaternary compounds of the Ag–Ga–S–AgBr system are described by the following equations:

$$\Delta_f G_{Ag_3Ga_2S_4Br}/\left(\text{kJ mol}^{-1}\right) = -(722.0 \pm 10.2) - (33.4 \pm 0.4) \times 10^{-3}\, \text{T/K}, \tag{19}$$

$$\Delta_f G_{Ag_{27}Ga_2S_{12}Br_9}/\left(\text{kJ mol}^{-1}\right) = -(2443.1 \pm 31.7) - (377.3 \pm 4.9) \times 10^{-3}\, \text{T/K}. \tag{20}$$

Included in Table 5 values of $\Delta_f G^{\circ}_{Ag_3Ga_2S_4Br}$ and $\Delta_f G^{\circ}_{Ag_{27}Ga_2S_{12}Br_9}$ do not contradict the hypothetical reactions of the synthesis of quaternary compounds from binary phases under standard conditions:

$$Ag_2S + Ga_2S_3 + AgBr = Ag_3Ga_2S_4Br, \tag{R3}$$

Table 5 Values of standard ($T = 298$ K and $P = 10^5$ Pa) thermodynamic properties of selected compounds of the Ag–Ga–S–AgBr system

Phases	$-\Delta_f G^{\circ}$	$-\Delta_f H^{\circ}$	S°	References
	kJ mol^{-1}		J (mol K)$^{-1}$	
Ag	0	0	42.677	[35]
Ga	0	0	40.828	[35]
S	0	0	32.056	[35]
Br_2	0	0	152.210	[35]
GaS	204.685	209.200	57.739	[35]
Ga_2S_3	505.702	516.306	142.256	[35]
AgBr	97.095	100.575	107.110	[35]
Ag_3SBr	132.0 ± 0.6	117.0 ± 0.4	50.2 ± 0.6	[36]
$Ag_3Ga_2S_4Br$	731.9 ± 8.9	722.0 ± 10.2	447.4 ± 5.8	Present study
$Ag_{27}Ga_2S_{12}Br_9$	2555.5 ± 28.4	2443.1 ± 31.7	2680.9 ± 34.9	Present study

Uncertainties for $\Delta_f G^{\circ}$, $\Delta_f H^{\circ}$, and S° are standard uncertainties

$$9Ag_2S + Ga_2S_3 + 9AgBr = Ag_{27}Ga_2S_{12}Br_9. \quad (R4)$$

Calculated values of the Gibbs energies of reactions (R3) and (R4) are equal, respectively: $\Delta_{r(R3)}G^\circ = -40.4\ \text{kJ mol}^{-1}$ and $\Delta_{r(R4)}G^\circ = -811.3\ \text{kJ mol}^{-1}$.

Conclusions

The phase space of the Ag–Ga–S–AgBr system in the GaS–Ga_2S_5–AgBr–Ag_2S part is characterized by the binary (Ag_2S, GaS, Ga_2S_3, AgBr), ternary (Ag_9GaS_6, $AgGaS_2$, Ag_3SBr), and quaternary ($Ag_3Ga_2S_4Br$, $Ag_{27}Ga_2S_{12}Br_9$) compounds. Quaternary compounds are components of the concentration tetrahedra GaS–Ga_2S_3–AgBr–$Ag_3Ga_2S_4Br$ and GaS–AgBr–$Ag_{27}Ga_2S_{12}Br_9$–$Ag_3Ga_2S_4Br$. The spatial position of the established tetrahedra relative to the silver point was used to establish the overall potential-determining reactions of the synthesis of compounds. The synthesis of quaternary compounds was carried out from the calculated amounts of binary phases in the positive electrodes of the cells with the participation of the Ag^+ catalyst. For the first time, the values of standard thermodynamic functions (Gibbs energies, enthalpies, and entropies) of quaternary compounds were calculated based on the temperature dependences of the EMF of electrochemical cells. The variation of the composition of ternary and quaternary compounds within the homogeneity regions opens wide possibilities for changing their physicochemical properties.

Acknowledgements The present work was financed partially by the grant of the Ministry of Education and Science of Ukraine No 0123U101857 "Physico-chemistry of functional nanomaterials for electrochemical systems", international projects: #HX-010123 from "Materials Phases Data System, Viznau, Switzerland" and the Simons Foundation (Award Number: 1037973). This work was partly funded by the K.H. Renlund Foundation under the project "Innovative e-waste recycling processes for greener and more efficient recoveries of critical metals and energy" at Åbo Akademi University.

Conflict of Interest
The authors declare that they have no conflict of interest.

References

1. Moroz M, Tesfaye F, Demchenko P, Prokhorenko M, Prokhorenko S, Reshetnyak O (2021) Non-activation synthesis and thermodynamic properties of ternary compounds of the Ag–Te–Br system. Thermochim Acta 698:178862(1)–(7). https://doi.org/10.1016/j.tca.2021.178862
2. Moroz M, Tesfaye F, Demchenko P, Kordan V, Prokhorenko M, Mysina O, Reshetnyak O, Gladyshevskii R (2023) Synthesis, thermodynamic properties, and structural characteristics of multicomponent compounds in the Ag–Ni–Sn–S system. JOM 75:2016–2025. https://doi.org/10.1007/s11837-023-05784-9

3. Ivashchenko I, Kozak V, Gulay L, Olekseyuk I (2022) Crystal structure of $AgGa_2Se_3Cl(Br)$ compounds. Proc Shevchenko Sci Soc Ser Chem Sci LXX:62–68. https://doi.org/10.37827/ntsh.chem.2022.70.062
4. Range K-J, Handrick K (1988) Neue 1320637-Verbindungen/New 1320637 compounds. Z Naturforsch B 43:240–242. https://doi.org/10.1515/znb-1988-0218
5. Brandt G, Krämer V (1976) Phase investigations in the silver-gallium-sulphur system. Mater Res Bull 11:1381–1388. https://doi.org/10.1016/0025-5408(76)90049-0
6. Chbani N, Loireau-Lozac'h A-M, Rivet J, Dugué J (1995) Système pseudo-ternaire Ag_2S-Ga_2S_3-GeS_2: diagramme de phases—domaine vitreux. J Solid State Chem 117:189–200. https://doi.org/10.1006/jssc.1995.1262
7. Ibragimova GI, Shikhiyev YuM, Babanly MB (2006) Solid phase equlibria in Ag-Ga-S (Se, Te) systems and thermodynamic properties of ternary phases. Chem Probl 1:23–28
8. Lin S, Li W, Bu Z, Gao B, Li J, Pei Y (2018) Thermoelectric properties of Ag_9GaS_6 with ultralow lattice thermal conductivity. Mater Today Phys 6:60–67. https://doi.org/10.1016/j.mtphys.2018.09.001
9. Hellstrom E, Schoonman J (1980) Silver ionic and electronic conductivity in Ag_9GaS_6. Solid State Ionics 1:199–210. https://doi.org/10.1016/0167-2738(80)90004-1
10. Lin S, Li W, Pei Y (2021) Thermally insulative thermoelectric argyrodites. Mater Today 48:198–213. https://doi.org/10.1016/j.mattod.2021.01.007
11. Asadov MM, Mustafaeva SN (2015) X-ray dosimetry of an $AgGaS_2$ single crystal. Bull Russ Acad Sci Phys 79:1113–1117. https://doi.org/10.3103/S106287381509004X
12. Laksari S, Chahed A, Abbouni N, Benhelal O, Abbar B (2006) First-principles calculations of the structural, electronic and optical properties of $CuGaS_2$ and $AgGaS_2$. Comput Mater Sci 38:223–230. https://doi.org/10.1016/j.commatsci.2005.12.043
13. Mouacher R, Seddik T, Rezini B, Haq B, Batouche M, Ugur G, Ugur S, Belfedal A (2022) First-principles calculations of electronic and optical properties of $AgGa_{1-x}Tl_xS_2$ alloys: analyses and design for solar cell applications. J Solid State Chem 309:122996. https://doi.org/10.1016/j.jssc.2022.122996
14. Palazon F (2022) Metal chalcohalides: next generation photovoltaic materials? Sol RRL 6:2100829. https://doi.org/10.1002/solr.202100829
15. Piasecki M, Myronchuk GL, Parasyuk OV, Khyzhun OY, Fedorchuk AO, Pavlyuk VV (2017) Synthesis, structural, electronic and linear electro-optical features of new quaternary $Ag_2Ga_2SiS_6$ compound. J Solid State Chem 246:363–371. https://doi.org/10.1016/j.jssc.2016.12.011
16. Kim J-H, Kim B-Y, Jang E-P, Yoon S-Y, Kim K-H (2018) Synthesis of widely emission-tunable Ag–Ga–S and its quaternary derivative quantum dots. Chem Eng J 347:791–797. https://doi.org/10.1016/j.cej.2018.04.167
17. Wei J, Hu Z, Zhou W, Qiu Y, Dai H (2021) Emission tuning of highly efficient quaternary Ag-Cu-Ga-Se/ZnSe quantum dots for white light-emitting diodes. J Colloid Interface Sci 602:307–315. https://doi.org/10.1016/j.jcis.2021.05.110
18. Azhniuk Y, Lopushanska B, Selyshchev O, Havryliuk Y, Pogodin A (2022) Synthesis and optical properties of Ag–Ga–S quantum dots. Phys Status Solidi B 259:2100349. https://doi.org/10.1002/pssb.202100349
19. Valakh M, Litvinchuk AP, Havryliuk Y, Yukhymchuk V, Dzhagan V (2023) Raman- and infrared-active phonons in nonlinear semiconductor $AgGaGeS_4$. Crystals 13:148. https://doi.org/10.3390/cryst13010148
20. Thirumoorthy M, Ramesh K (2021) Characteristics of pulse electrodeposited $AgGaS_2$ thin films for photovoltaic application. Mater Today Proc 47:1847–1854. https://doi.org/10.1016/j.matpr.2021.03.410
21. Moroz MV, Demchenko PYu, Prokhorenko MV, Reshetnyak OV (2017) Thermodynamic properties of saturated solid solutions of the phases Ag_2PbGeS_4, $Ag_{0.5}Pb_{1.75}GeS_4$ and $Ag_{6.72}Pb_{0.16}Ge_{0.84}S_{5.20}$ of the Ag-Pb-Ge-S system determined by EMF method. J Phase Equilibria Diffus 38:426–433. https://doi.org/10.1007/s11669-017-0563-6

22. Moroz MV, Prokhorenko MV, Reshetnyak OV, Demchenko PYu (2017) Electrochemical determination of thermodynamic properties of saturated solid solutions of Hg_2GeSe_3, Hg_2GeSe_4, $Ag_2Hg_3GeSe_6$, and $Ag_{1.4}Hg_{1.3}GeSe_6$ compounds in the Ag–Hg–Ge–Se system. J Solid State Electrochem 21:833–837. https://doi.org/10.1007/s10008-016-3424-z
23. Moroz MV, Demchenko PYu, Mykolaychuk OG, Akselrud LG, Gladyshevskii RE (2013) Synthesis and electrical conductivity of crystalline and glassy alloys in the Ag_3GeS_3Br-GeS_2 system. Inorg Mater 49:867–871. https://doi.org/10.1134/S0020168513090100
24. Moroz MV, Prokhorenko MV (2014) Thermodynamic properties of the intermediate phases of the Ag-Sb-Se system. Russ J Phys Chem A 88:742–746. https://doi.org/10.1134/S0036024414050203
25. Moroz M, Tesfaye F, Demchenko P, Prokhorenko M, Lindberg D, Reshetnyak O, Hupa L (2018) Phase equilibria and thermodynamics of selected compounds in the Ag–Fe–Sn–S system. J Electron Mater 47:5433–5442. https://doi.org/10.1007/s11664-018-6430-3
26. Moroz MV, Prokhorenko MV, Rudyk BP (2014) Thermodynamic properties of phases of the Ag-Ge-Te system. Russ J Electrochem 50:1177–1181. https://doi.org/10.1134/S1023193514120039
27. Prokhorenko MV, Moroz MV, Demchenko PYu (2015) Measuring the thermodynamic properties of saturated solid solutions in the Ag_2Te-Bi-Bi_2Te_3 system by the electromotive force method. Russ J Phys Chem A 89:1330–1334. https://doi.org/10.1134/S0036024415080269
28. Moroz M, Tesfaye F, Demchenko P, Prokhorenko M, Kogut Y, Pereviznyk O, Prokhorenko S, Reshetnyak O (2020) Solid-state electrochemical synthesis and thermodynamic properties of selected compounds in the Ag–Fe–Pb–Se system. Solid State Sci 107:106344(1)–(9). https://doi.org/10.1016/j.solidstatesciences.2020.106344
29. Babanly M, Yusibov Y, Babanly N (2011) The EMF method with solid-state electrolyte in the thermodynamic investigation of ternary copper and silver chalcogenides. In: Kara S (ed). InTech, pp 57–78. https://doi.org/10.5772/28934
30. Mammadov FM, Amiraslanov IR, Imamaliyeva SZ, Babanly MB (2019) Phase relations in the FeSe–$FeGa_2Se_4$–$FeIn_2Se_4$ system: refinement of the crystal structures of $FeIn_2Se_4$ and $FeGaInSe_4$. J Phase Equilibria Diffus 40:787–796. https://doi.org/10.1007/s11669-019-00768-2
31. Hasanova GS, Aghazade AI, Babanly DM, Imamaliyeva SZ, Yusibov YA, Babanly MB (2021) Experimental study of the phase relations and thermodynamic properties of Bi-Se system. J Therm Anal Calorim 147:6403–6414. https://doi.org/10.1007/s10973-021-10975-0
32. Gravetter FJ, Wallnau LB (2017) Statistics for the behavioral sciences, 10th edn. Cengage Learning, Australia and United States
33. Babanly NB, Orujlu EN, Imamaliyeva SZ, Yusibov YA, Babanly MB (2019) Thermodynamic investigation of silver-thallium tellurides by EMF method with solid electrolyte Ag_4RbI_5. J Chem Thermodyn 128:78–86. https://doi.org/10.1016/j.jct.2018.08.012
34. Imamaliyeva SZ, Musayeva SS, Babanly DM, Jafarov YI, Taghiyev DB, Babanly MB (2019) Determination of the thermodynamic functions of bismuth chalcoiodides by EMF method with morpholinium formate as electrolyte. Thermochim Acta 679:178319. https://doi.org/10.1016/j.tca.2019.178319
35. Barin I (1995) Thermochemical data of pure substances. VCH, Weinheim
36. Moroz MV, Prokhorenko MV, Prokhorenko SV (2015) Determination of thermodynamic properties of Ag_3SBr superionic phase using EMF technique. Russ J Electrochem 51:886–889. https://doi.org/10.1134/S1023193515090098